Infrared Face Vascular ID: Vascular structure matching algorithm

Aasminpreet Singh Kainth
Department of Computer Science
Middlesex College, University of Western Ontario
London, Ontario, Canada.
akainth4@uwo.ca

Abstract – ***Major approaches to face authentication systems rely on facial characteristics over the skin. Some of these characteristics can be altered, and their phenomenology varies significantly with environmental factors*** [1] ***(e.g., lighting). Whereas research in vascular structure inside our skin is attaining attention due to simple and contact free capture. The aim behind this effort is to find the possibility of using these structures in authentication method. In this paper, Biometric Graph Comparison technique is used to match the vascular structures of the face. This technique is comprised of graph registration and graph matching of structures detected in vascular graph. These structures are traced and rotated then compared their distance measure based on the number of vertices or edges in the maximum common subgraph. The research shows the benefits of graph representation for facial vascular biometrics and the advantages of graph topology in matching vascular biometric graphs.*** [2] ***The obtained results strengthen the feasibility of face vascular graph structure matching and open the way for further methodological and experimental research in the area.***

I. Introduction

With advent of time, passwords, PINs and hardware tokens keep failing and the demand of new passwordless authentication keeps on rising. The race to find the new authentication scheme between the researchers is up since the last decade and each of them each of them presented their own pros and cons. One such authentication system is the biometric system which depends on the "who we are" factor in which the physical and biological characteristics of a person such as speech, iris, thumb impressions or face are used for authentication. The fingerprint biometrics [3] are widely used as of now, but they do have many disadvantages such as the imitation of fingerprint using a sticky tape [4]. Also, the case of wear and tear of fingerprints as a part of natural aging is also problematic. Efficiency of Apple's face ID [5] is also a popular tech discussion these days as of COVID situations people are facing difficulty in getting their face ID access wearing the mask. Additionally, natural aging, change of expression, presence and absence of facial hair or spectacles adds up to unreliability in face authentication systems. There is also the matter of false positives, where a biometric authentication system incorrectly grants authorization to an individual that isn't the intended user — a problem that is more likely among twins or sometimes even family members (though Face ID's false positive rate is reportedly about one in a million) [6].

For the above reasons, vein pattern recognition has been growing in popularity in recent months, both for the advanced security it promises, but also because of the contactless use cases it offers, a point especially popular these days due to the rise of COVID-19 and concerns about commonly touched surfaces like those found on many hand and

fingerprint scanners. Human vein patterns are found to be unique even in the case of twins. Adding on to it, Apple [7] filed a patent recently that looks to improve upon facial recognition methodology by mapping the unique vein patterns beneath a person's face. The patent — titled "Vein matching for difficult biometric authentication cases" [8] — calls for the use of an infrared sensor to capture subcutaneous (beneath the user's face) vein patterns in a 3D map, and then using the data from that map for authentication. Fig 1. Depicts a flowchart of an

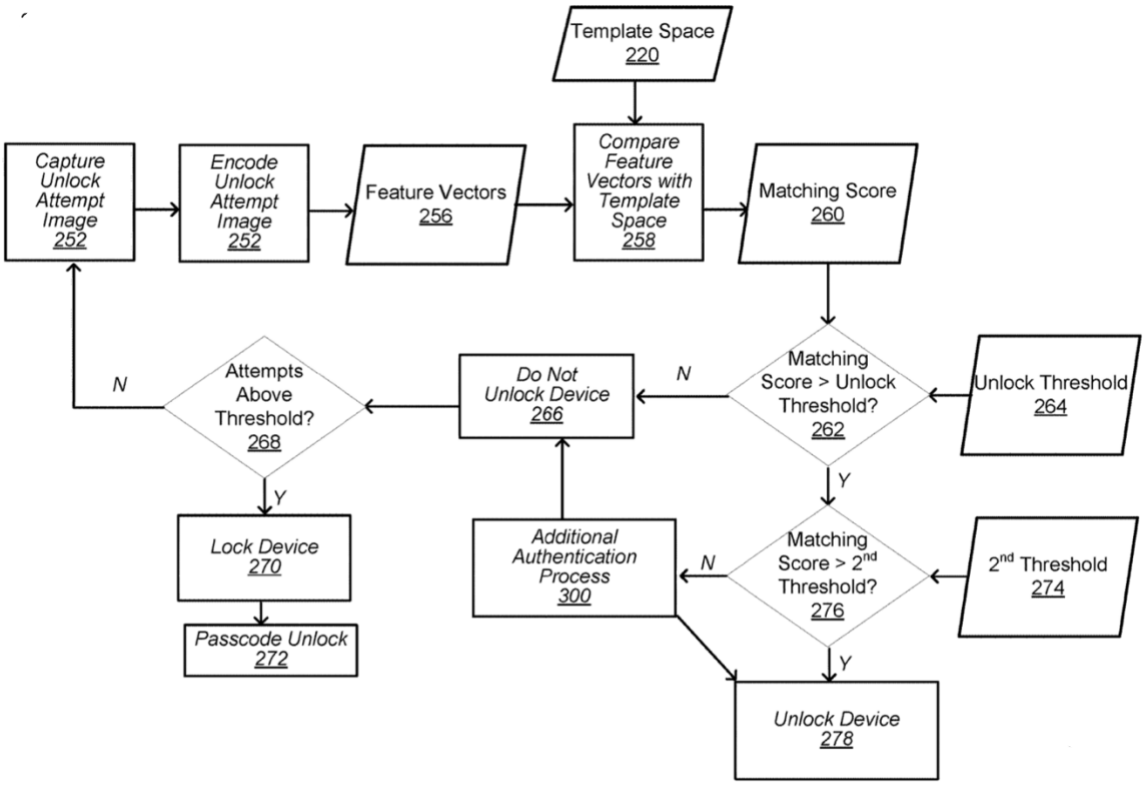

Figure 1 depicts a flowchart of an embodiment of facial recognition authentication process from Apple's patent. [8]

embodiment of facial recognition authentication process from the patent.

The subcutaneous vascular pattern i.e., the internal vascular structures cannot be seen under the normal light which makes it impossible to capture without the person's intent. Some research [9] which are working on retina vascularity or palm vein structures has shown the higher accuracy results paving the way to more secure future authentication schemes.

Infrared imaging is emerging and replacing the visible spectrum technology to some extent such as Apple [7] is using infrared sensor to sense the dot projected on the user's face to register and match with face ID. The notable benefit of thermal infrared data in comparison with conventional visible spectrum images in the context of face recognition lies in its invariance to visible spectrum illumination. [10]

The invariance property of IR data in comparison to visible spectrum illumination is the major advantage. Infrared energy is less affected by absorption and scattering by smoke or dust than visible spectrum light. [11] As to be the essential part of research the IR imaging can extract the under the skin vein structure which is impossible to do with visible spectrum light. Also, the IR imaging can detect the facial disguises.

Infrared spectrum is divided into various sub-IR spectrum according to wavelength such as the NWIR, MWIR, LWIR, for which the LWIR and MWIR [12] spectrum is sensitive to the environmental temperature, as well as the health, and physical conditions of the subject [10]. Even the emotional condition of the subject too can be

detected. The loss of important information is observed if the subject wears the eyeglasses which are opaque to IR waves. Impact of sunlight persist if capturing of the subject image takes place outdoors. Though invariant to the changes in the illumination by visible light itself, the infrared "appearance" in the SWIR sub-bands is affected by sunlight which has significant spectral components at the corresponding wavelengths. [10] [10] [12]

Motivation:

Although it is essential to develop a long-term authentication strategy, Verizon believe that the next digital breakthrough will be passwordless authentication, mainly for security reasons, but the reasons are not limited to this.

The rest of the paper is organized as follows. Section 2 provides the background information of the papers read. The discussion to research is presented in Section 3, while Section 4 aims to conclude and Section 5 mentions the future work. Section 6 gives references to research papers discussed.

II. BACKGROUND

Initially, the [13] work done by Prokoski et al. in 1992 started working on to look for the potential in infrared imaging for face recognition. Before then automatic methods which were used by visible spectrum imaging were followed to closely mirrored the results obtained by IR thermal imaging. The simple statistical methods were used to extract the holistic face presence, with little attempt to achieve any generalization.

Later attempts to extract useful information from under the skin by IR imaging is done by Wu et al. [14]

They used a series of assumptions on relative temperatures of body and superficial tissue, the formulated differential equation leading blood perfusion is the following

Equation 1 defines the thermogram to blood perfusion transform [14]

$$\omega = \frac{\varepsilon\sigma(T_s^4 - T_e^4) + A\mu d^{3M-1}(\mathrm{P}\, g\beta/\nu^2)^M (T_s - T_e)^{M+1} - k(T_c - T_s)/D - H_m}{\alpha c_b (T_a - T_s)}$$

where the specific parameters are tabulated in Table 1.

symbol	description	Value
ω	Blood perfusion	
σ	Stefan-Boltzmann constant	$5.67*10^{-8}$ W $m^{-2}K^{-4}$
ε	Tissue/ skin thermal emissivity	0.98
T_s	Skin temperature	
T_e	Ambient temperature	
T_a	Artery temperature	312.15K
T_c	Core temperature	312.15K
k	tissue/ skin thermal conductivity	$0.2Wm^{-1}K^{-1}$
μ	Air thermal conductivity	0.024 W $m^{-1}K^{-1}$
c_b	blood specific heat	$3.78*10^3$ Jkg^{-1} K^{-1}
H_m	metabolic heat flux per unit area	4.186W m^{-2}
α	tissue/ skin countercurrent exchange ratio	0.8
P	Prandtl constant	0.72
ν	kinematic viscosity of air	$1.56*10^{-5}$ m^2/ s
β	air thermal expansion coefficient	$3.354*10^{-3}K^{-1}$
g	local gravitational acceleration	9.8m^2/ s
A	constant	0.27
M	constant	0.25
d	Characteristic length of a face	0.095
D	Distance from body core to skin surface	0.095

Table 1 Nomenclature [14]

Using this model, from the original segmented facial image a "blood perfusion image" is then computed which thereafter is matched using a standard linear discriminant.

(a) Thermal data (T_e = 26.2°C); (b) Corresponding blood perfusion data

Figure 2 Thermal data vs blood perfusion data (method of Wu et al.)

Then Buddharaju et al. [15] [16] explored the use of anatomical feature which is considered the most prominent method till date, some of the key observations behind their research displays that blood vessels are slightly warmer than the surrounding tissues, allowing them to be identified in thermograms [10] [15]. These temperature differences are cannot be observed or seen with the naked eye as the differences are very small. Another important observation which bolsters the research in

facial vein authentication is that the blood vessels are "hardwired" at birth and remain unaffected by factors such as aging, except any physical injury [17].

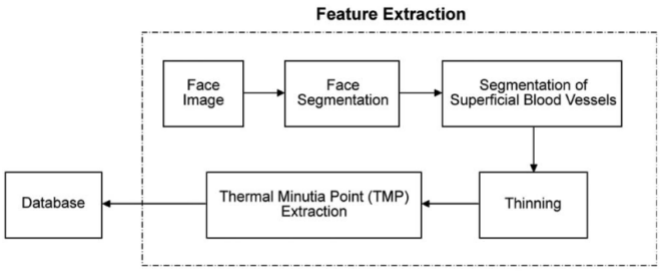

Figure 3 Architecture of feature extraction algorithm from Buddharaju et al. method [1]

There are some series of background-foreground segmentation steps of a face which are followed by extraction of blood vessels from an image using simple morphological filters in the methods of Buddharaju et al. To localize salient feature of the network, the skeletonized vascular network is used. These salient features are also termed as thermal minutia points which are similar in nature to the minutia points used in fingerprint recognition. [18]

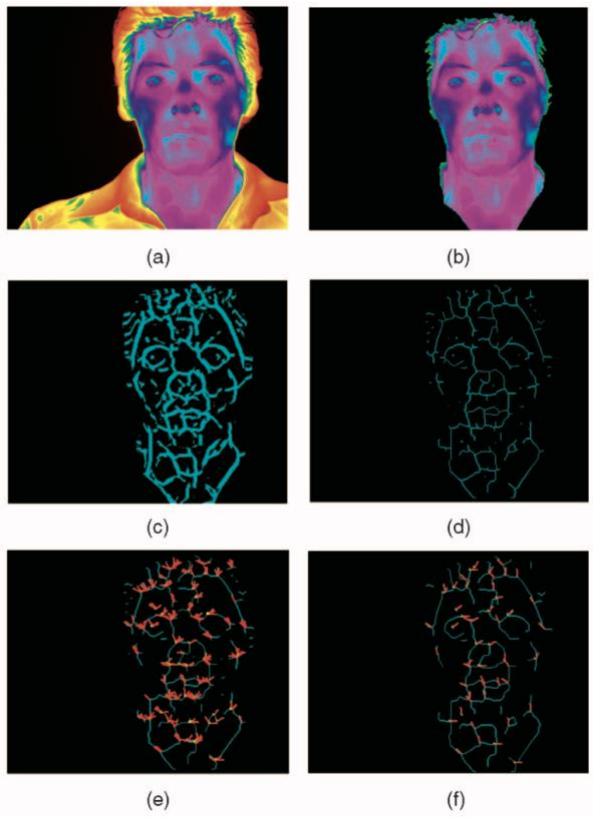

Figure 4 Visualization of the various stages of the vascular feature extraction algorithm [1]

In Buddharaju's method, they used a popular fingerprint recognition method i.e., by matching the sets of minutia points using relative minutiae orientations on local and global scale [10]. Matching is a two-step process (as shown in fig 5):

1. vascular network of the test is registered with the database subjects using the dual bootstrap ICP Algorithm

2. to generate matching score. Score is generated by pixel-to-pixel comparison of the test and database vascular networks.

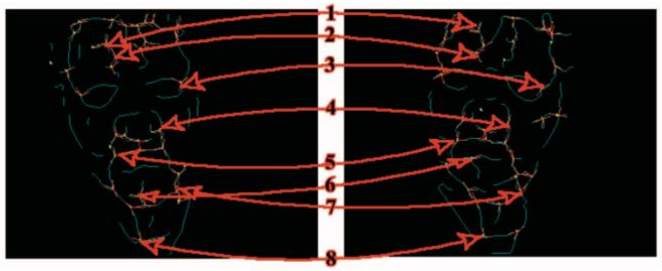

Figure 5 Matching of Thermal Minutia Points

There are some problems with Buddharju's method such as they used a simple heuristic pixel to pixel comparison for the matching algorithm that compares the registered network of test and database subject. Their results are based on a binary image where pixel either belongs or does not belong to the vascular network which makes it sensitive to variable pose changes [10] of the face or the change in the facial expression for which they trained their algorithm multiple images with different pose. In their research they have not mentioned anywhere about the results facial recognition matching after a certain period of time which could point a question to their results as of the uncertainty for the output of the pixels. This might have an intense consequence in the performance of their system. The output produced is sensitive to the scale of the face which makes it difficult in matching the results with the distance change of the user's face from the camera. Lastly, eyeglasses issue is problematic as they compared the people with eyeglasses as it is without making them remove it as a large portion of subject vessels get opaque to IR waves.

Some research questions arise to work on these problems such as How can we extract vascular network which gives invariable matching result to the distance changes, pose changes and facial expression changes? Or is there any way to normalize the facial expression and pose in thermal faces using some complex models?

III. Discussion

Biometric Graph Extraction

In 2011, 'biometric graph' term is coined which means a 3-dimensional graph with blood vein feature of crossovers (where two veins appear to intersect in the skeleton), bifurcations (where one vein splits into two) or terminations (where the veins go out of the frame of reference) forming the graph [19]. Two vertices can form an edge between them after tracing a line along the vein from one end to other. Fig. 6 shows examples of biometric graphs from the four different modalities which are the palm, wrist, hand and retina. [20]

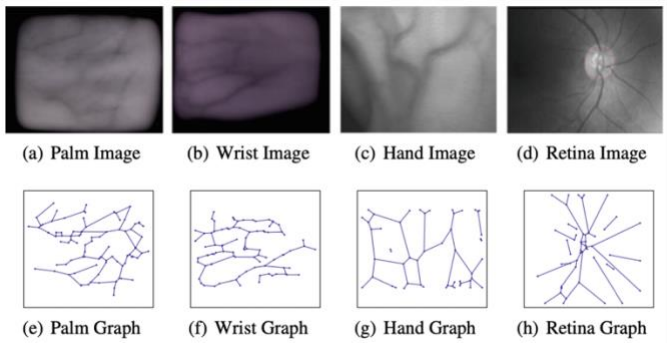

Figure 6 Spatial Graphs of 4 different modalities i.e. Palm, Hand, Retina and Wrist

To construct a bio graph from 2D image, vascular skeleton is extracted, and the feature points are found which are labelled to form the vertex set, and their coordinates are recorded. By tracing the skeleton from each feature point to another the existence of an edge between vertices is determined where the length and slope is calculated and stored, additionally other feature points and vessel segment attributes can be calculated at the same time. [2]

In figure 7, example of graphs extracted from the palm vein vascular biometric modality is given for which the red circle shows an example of a claw structure, and the red square shows an example of a two-claw structure which is formed by a pair of star structures sharing a common edge. [20]

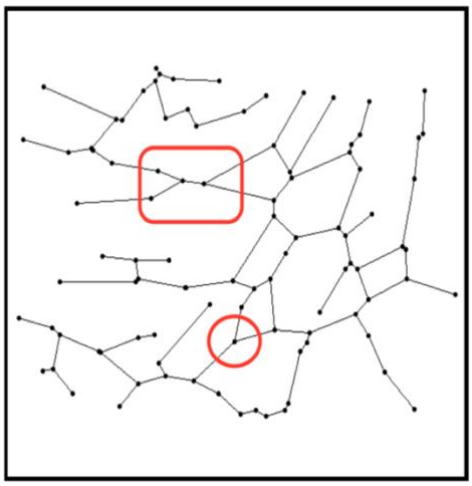

Figure 7 Vascular biometric graphs extraction

Biometric Graph Matching Algorithm

The algorithm is divided into two parts: **Biometric Graph Registration** which requires 4 steps and **Biometric Graph Comparison** which has 3 steps. The four parameters that define our registration algorithm are a vertex comparison tolerance ε, a structure S, a structure pair length L and a similarity score function f which depends on the structure selected. The structures S used are: Edges (E), Claws (C) and Two-claws (T). [2] [20]

Therefore, BGR (S, f, L, ε) is used to denote the algorithm

Step 1: In the beginning select S, f, L, ε. For the inputs take two graphs g and g', the process of registration begins identifying all the structures and then listing those structures of the selected types in each graph. [2]

Step 2: *Similarity scoring structure pairs*

Using the appropriate similarity structure function F, the similarity score is obtained by comparing the first structure from graph g with the second structure from graph g'.

Step 3: *Shortlisting structure pairs and aligning on them*

Ordering of the structure pairs takes place in the decreasing order of similarity score where the pairs get shortlisted for further processing. Translation and Rotation of every shortlisted structure pair is done so that a specific part of the structure becomes the origin of the reference frame.

Step 4: Pair alignment scoring and graph registration

Each vertex in the first graph is matched to the vertex of the second graph g' after aligning the graphs in the same coordinate system on a shortlisted pair. It will only be matched a vertex in g find a corresponding vertex in g' within ε pixels of it.

Then *QuickScore* (QS) is calculated via the total number of matched vertices after normalizing it by the geometric mean of the number of vertices in two graphs.

That is, if g has n vertices, g′ has n′ vertices and the aligned graphs have c matched vertices within tolerance ε, the distance between g and g′ is calculated to be

$$QS(g,\ g') = 1\ - \frac{c}{\sqrt{n \times n'}}$$

The smallest score obtained from the pair of structures is chosen to register g and g'. The resulting registered graphs are denoted g_a and g'_a.

From the above example in figure 8 it is observed that registration with two-claw structure gave a larger number of matched vertex pairs than the claw structure.

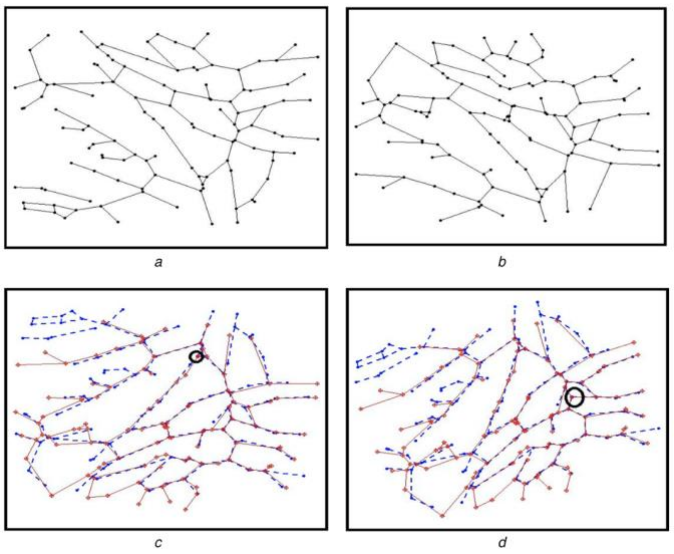

Figure 8 Fig. Pain Vein registration graphs in (a) and (b). The bottom figures show registration using (c) the two-claw structure and (d) the claw structure.

BGC-Biometric Graph Comparison

Hungarian algorithm-based method proposed by Risen and Bunke [21] can be used to compare the graphs after the graphs get registered.

BG comparison algorithm has three steps:

1. determination of the minimum graph edit path between g_a and g'_a
2. construction of the Maximum Common Subgraph (MCS) of g_a and g'_a
3. measurement of the difference between g_a and g'_a using the MCS.

Conversion of different graphs can be done via three operations - insertions of features, deletions of features and substitutions of features and have associated costs. [19]

An *optimisation algorithm* is then used which makes use of cost matrix, which is used for the selection of right costs of these substitutions, insertions and deletions operations to achieve a significant measure of distance. The output of this algorithm will be a list of edit operations that give the lowest cost. Four different cost matrices based on the different structures are formed for which larger the number of features in each pair of graphs, the bigger will be the matrices and the longer it will take the Hungarian algorithm to compute the optimum result. [22]

IV. Conclusion

The matching algorithm that is proposed could provide better recognition accuracy [10] compared to point pattern approaches from the previous works. BG registration plays the key role of the algorithm efficiency as it helps in achieving the better similarity score and helps in minimising the number of false non-matches. The capture mechanism plays a critical role as the approximate distance, pose and tilted camera position can make the large difference in the registration of the graph. Also, the time between each capture gives seldom equal results unless both the registered graph and the graph in the database are aligned well making the comparison perfect.

Therefore, if registration is not done properly [10], the graphs will be in different reference frames. Hence, in accurately bringing both the graphs to same reference, the BG registration process plays the major role. Increase in the false reject rate will be observed while the graph matching process. The matching algorithm that is proposed can provide better recognition accuracy compared to point pattern approaches from the previous works.

As the output produced by Buddharaju's approach [1] is very sensitive to the scale of the face and thus **lacks robustness** to the distance of the user from the camera but with the Biometric registration strategy proposed it can be solved. [2] Also, Buddharaju et al. [15] results are **sensitive to variable pose,** the BGM can solve this problem too.

So, if biometric graph matching algorithm proposed in this paper is used in face vascular authentication systems, it might increase the accuracy of registration and can also improve the similarity scores from over single structures to better results from variable structures such as claws, two claws and edges.

V. Future Work

The followings are suggested as future work:

1. Examining the scalability of the system on larger and challenging databases which simulate more realistic conditions.
2. Testing the time robustness of the proposed system on a larger number of subjects after a long period of time.
3. Comparing the results of our vascular network with that of radiological images in order to determine those parts of the vascular network which correspond to the real vascular network.

VI. References

[1] P. Buddharaju, I. T. Pavlidis, P. Tsiamyrtzis and M. Bazakos, "Physiology-Based Face Recognition in the Thermal Infrared Spectrum," *IEEE,* vol. 29, no. 4, pp. 613 - 626, 2007.

[2] A. A. a. D. J. Horadam, "Vascular Biometric Graph Comparison: Theory and Performance," in *Handbook of Vascular Biometrics*, Open Access, 2019, pp. 355-393.

[3] S. Kirchgasser, C. Kauba, Y.-L. Lai, J. Zhe and A. Uhl, "Finger Vein Template Protection Based on Alignment-Robust Feature Description and Index-of-Maximum Hashing," *IEEE TRANSACTIONS ON BIOMETRICS, BEHAVIOR, AND IDENTITY SCIENCE,* vol. 2, no. 4, 2020.

[4] C. Sousedik and C. Busch, "Presentation attack detection methods for fingerprint recognition systems: a survey," *IET Biometrics,* 2013.

[5] Apple Inc., "About Face ID advanced technology," Apple Inc., 26 February 2020. [Online]. Available: https://support.apple.com/en-ca/HT208108. [Accessed 7 September 2020].

[6] J. Alghamdi, R. Alharthi, R. Alghamdi, W. Alsubaie, R. Alsubaie, D. Alqahtani and R. A. ramadan, "A Survey On Face Recognition Algorithms," *3rd International Conference on Computer Applications & Information Security (ICCAIS),* 2020.

[7] Apple Insider, "Apple Patent Would Add Vein Biometrics to Face ID," mobileidworld, 21 July 2020. [Online]. Available: https://mobileidworld.com/apple-patent-biometric-face-id-vein-recognition-072109/. [Accessed 21 August 2020].

[8] MicahP.Kalscheur and FengTang, " VEIN MATCHING FOR DIFFICULT BIOMETRIC AUTHENTICATION CASES". United States of America Patent US20190080153A1, 14 March 2019.

[9] M. Stanuch, M. Wodzinski and A. Skalski, "Contact-Free Multispectral Identity Verification System Using Palm Veins and Deep Neural Network," *MDPI,* 2020.

[10] R. S. Ghiass, O. Arandjelović, H. Bendada and X. Maldague, "Infrared face recognition: A literature review," *IEEE,* 4 Aug 2013.

[11] "Infrared Waves - Tour of the Electromagnetic Spectrum," National Aeronautics and Space Administration, Science Mission Directorate., 2010. [Online]. Available: http://science.nasa.gov/ems/07_infraredwaves. [Accessed 24 Sept 2020].

[12] From Wikipedia, the free encyclopedia, "Infrared spectroscopy," Wikipedia, [Online]. Available: https://en.wikipedia.org/wiki/Infrared_spectroscopy. [Accessed 13 September 2020].

[13] F. Prokoski and R. Riedel, "BIOMETRICS: Personal Identification in Networked Society," *IEEE,* 1998.

[14] S.-Q. Wu, W. Song, L.-J. Jiang, S. -L. Xie, F. Pan, W.-Y. Yau and S. Ranganath, "Infrared Face Recognition by Using Blood Perfusion Data," *International Conference on Audio- and Video-Based Biometric Person Authentication,* vol. 3546, pp. 320-328, 2005.

[15] P. Buddharaju and I. Pavlidis, "Physiological face recognition is coming of age," *IEEE Conference on Computer Vision and Pattern Recognition,* 2009.

[16] R. S. Ghiass, O. Arandjelović, H. Bendada and X. Maldague, "Illumination-invariant face recognition from a single image across extreme pose using a dual dimension AAM ensemble in the thermal infrared spectrum," *The 2013 International Joint Conference on Neural Networks (IJCNN),* 2014.

[17] A. B. Persson1 and I. R. Buschmann, "Vascular Growth in Health and Disease," *Front Mol Neurosci.,* 2011.

[18] H. Xu, R. N. J. Veldhuis, A. M. Bazen, T. A. M. Kevenaar, T. A. H. M. Akkermans and B. Gokberk, "Fingerprint Verification Using Spectral Minutiae Representations," *IEEE Transactions on Information Forensics and Security,* vol. 4, no. 3, pp. 397 - 409, 2009.

[19] S. M. Lajevardi, A. Arakala, S. Davis and K. J. Horadam, "Hand vein authentication using biometric graph matching," *IET Biometrics,* 2014.

[20] A. Arakala, S. A. Davis1, H. Hao and K. J. Horadam, "Value of graph topology in vascular biometrics," *IET Biometrics,* 2016.

[21] K. Riesen and H. Bunke, GRAPH CLASSIFICATION AND CLUSTERING BASED ON VECTOR SPACE EMBEDDING, Singapore: World Scientific Publishing Co. Pte. Ltd., 2010.

[22] F. LIU, S. JIANG, B. KANG and T. HOU, "A Recognition System for Partially Occluded Dorsal Hand Vein Using Improved Biometric Graph Matching," *IEEE,* 2020.

VII. Appendix

Algorithm 1: Graph registration module

Require: Graphs g and g' with vertex sets $\mathbf{V}=\{v_1, v_2, \cdots, v_m\}$ and $\mathbf{V'}=\{v'_1, v'_2, \cdots, v'_{m'}\}$ and vertex sets $\mathbf{E}=\{e_1, e_2, \cdots, e_n\}$ and $\mathbf{E'}=\{e'_1, e'_2, \cdots, e'_{n'}\}$ respectively. Let L be the number of structure pairs to shortlist and let ε be the tolerance to match vertex pairs.

Ensure: Aligned graphs g_a and g'_a having same vertex links as g and g' but with new spatial coordinates.

$g_a \leftarrow \varnothing$ and $g'_a \leftarrow \varnothing$. ▷ Initialise the registered graphs that will be returned at the end of the algorithm

$\mathbf{S} = \{ s_1, s_2, \cdots, s_n \}$ is the list of structures in g.
$\mathbf{S'} = \{ s'_1, s'_2, \cdots, s'_{n'} \}$ is the list of structures in g'.
$M_{dist} \leftarrow 0$ ▷ Initialise a matrix of size $n \times n'$ with zeros.
for $a = 1$ to n **do**
  for $b = 1$ to n' **do**
    $d_{ab} = \text{StructDist}(s_a, s_b, F)$ ▷ This function returns the distance between the two structures. The flag F indicates if the structure is an vertex, star or two-star.
    $M_{dist}[a,b] \leftarrow d_{ab}$
  end for
end for

Sort the contents of M_{dist} in increasing order.
$M_{shortlist}$ is a matrix with 3 columns.
Every row m_i stores the 3-tuple (d_{abi}, a_i, b_i).
d_{abi} is taken from the sorted M_{dist} with the first row of $M_{shortlist}$, m_1 having d_{ab1}, the smallest distance.
a_i and b_i indicate the corresponding row and column of d_{abi} in M_{dist}.

$d_{struct} \leftarrow (0,0,\cdots,0)_{1\times L}$ ▷ A vector to store the distances between graphs when aligned on each of the shortlisted structure pairs
for $i = 1$ to L **do**
  $a = a_i$, $b = b_i$ where $m_i \in M_{shortlist}$
  $g_o = \text{TransRot}(g, e_a)$. ▷ Translate and rotate g with respect to the specific vertex in the shortlisted structure
  $g'_o = \text{TransRot}(g', e'_b)$.
  $d_{struct}[i] = \text{QuickScore}(\, g_o, g'_o, \varepsilon\,)$ ▷ Compute a distance based on vertex correspondence between the translated and rotated graphs
end for

$d_{min} = \text{MIN}\,(\, d_{struct}\,)$.
a_{min} and b_{min} are the row and column in $M_{shortlist}$ corresponding to d_{min}.
$g_a = \text{TransRot}(g, e_{a_{min}})$.
$g'_o = \text{TransRot}(g', e'_{b_{min}})$.
return g_a, g'_a and d_{min}.

function $\text{EucDist}(\, A=(a_1,a_2,\cdots,a_z)\,,\, B=(b_1,b_2,\cdots,b_z)\,)$
  $d = \sqrt{(a_1-b_1)^2+(a_2-b_2)^2+.....(a_z-b_z)^2}$ **return** d
end function

function $\text{StructDist}(s_a, s_b, F)$ $d_{structPair} \leftarrow \varnothing$
  if F ==“vertex” **then**
    $V_a \leftarrow (l_a, \theta_a)$ ▷ The length and slope of the vertex
    $V_b \leftarrow (l'_b, \theta'_b)$
    $d_{structPair} = \frac{1}{0.5(l_a+l'_b)}\text{EucDist}(V_a, V_b)$ ▷ The Euclidean distance between the lengths l and l' and slopes θ and θ' of the vertex pair.
  end if
  if F ==“star” **then**
    $L_a \leftarrow (l_{1a}, l_{2a}, l_{3a})$ ▷ The three vertices of the star in decreasing order of length
    $\Theta_a \leftarrow (\theta_{12a}, \theta_{23a})$ ▷ The angles between first and second vertex and the second and third vertex.
    $L'_b \leftarrow (l'_{1b}, l'_{2b}, l'_{3b})$
    $\Theta_b \leftarrow (\theta'_{12b}, \theta'_{23b})$
    $l_\delta \leftarrow \text{EucDist}(L_a, L'_b)$
    $a_\delta \leftarrow \text{EucDist}(\Theta_a, \Theta'_b)$
    $d = l_\delta + a_\delta$
    $d_{structPair} = d$
  end if
  if F ==“two-star” **then** ▷ A two-star has two-star structures connected by a common vertex
    $L_a \leftarrow (l_{1a}, l_{2a}, l_{3a}, l_{4a}, l_{5a}, l_{6a})$ ▷ l_1 and l_4 are the longest vertices of the first and second star structures. The other two vertex follow the longest vertex in decreasing order of length.
    $\Theta_a \leftarrow (\theta_{12a}, \theta_{23a}, \theta_{45a}, \theta_{56a})$ ▷ The four internal angles, two each from each of the two-stars.
    l_{*a} is the length of the connecting vertex between the two-stars in structure a where $* \in \{1,2,3,4,5,6\}$.
    $L'_b \leftarrow (l'_{1b}, l'_{2b}, l'_{3b}, l'_{4b}, l'_{5b}, l'_{6b})$
    $\Theta'_b \leftarrow (\theta'_{12b}, \theta'_{23b}, \theta'_{45b}, \theta'_{56b})$
    l'_{*b} is the length of the connecting vertex between the two-stars in structure b where $* \in \{1,2,3,4,5,6\}$.
    $d_1 = \text{EucDist}(\, L_a[1:3]\,,\, L'_b[1:3]) + \text{EucDist}(\Theta_a[1:3]\,,\, \Theta'_b[1:3]\,)$
    $d_2 = \text{EucDist}(\, L_a[4:6]\,,\, L'_b[4:6]\,) + \text{EucDist}(\Theta_a[4:6]\,,\, \Theta'_b[4:6])$
    $d_3 = \text{EucDist}(\, l_{*a}, l'_{*b}\,)$.
    $d_{structPair} = d_1 + d_2 + d_3$
  end if
  return $d_{structPair}$
end function

function $\text{TransRot}(g, e\,)$
  $g_o \leftarrow g$
  The start vertex of e will be the origin of the coordinate system.
  The vertex e will be define the positive direction of the x-axis.
  Recalculate all the vertex attributes of g_o in the new coordinate system. **return** g_o.
end function

function $\text{QuickScore}(g, g', \varepsilon)$
  Label all vertices of g and g' as unmatched.
  $C = 0$ ▷ Counter for number of vertex pair matches between g and g'
  for $i = 1$ to m **do**
    for $j = 1$ to m' **do**
      if v_i is labeled unmatched and v'_j is labeled unmatched and EUCDIST(q_i, q'_j) $\leq \varepsilon$ **then**
        $C = C + 1$. ▷ v_i matches with v'_j.
        Label v_i and v'_j as matched. ▷ $q_i = (q_{1i}, q_{2i})$ is the vertex attribute of v_i and q'_i is the vertex attribute of v'_i .
      end if
    end for
  end for
  $d = 1 - \frac{C}{\sqrt{m \times m'}}$. **return** d.
end function